Short Article

Structure

An Unexpected Duo: Rubredoxin Binds Nine TPR Motifs to Form LapB, an Essential Regulator of Lipopolysaccharide Synthesis

Graphical Abstract

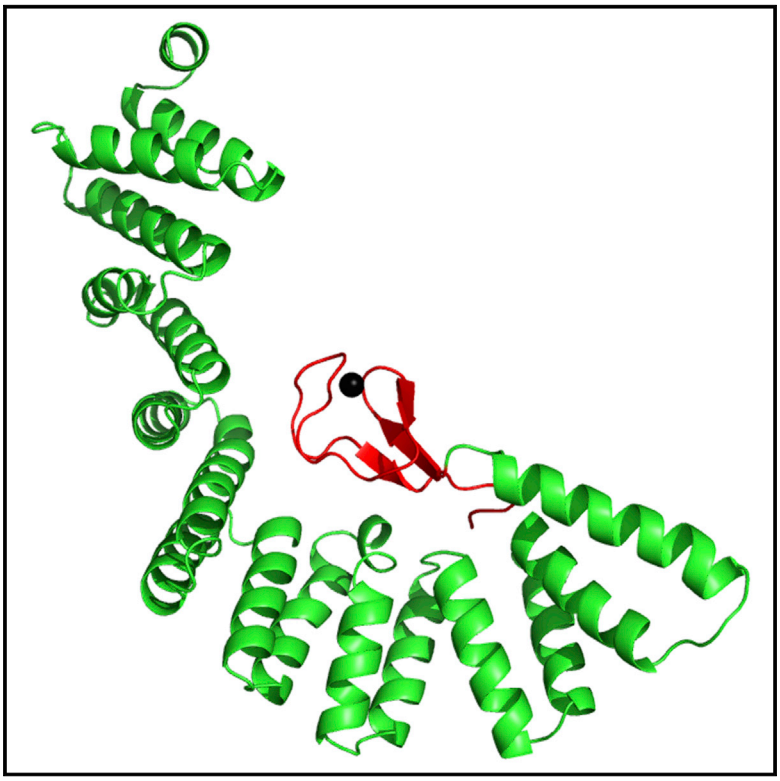

Authors

Chelsy Prince, Zongchao Jia

Correspondence

jia@queensu.ca

In Brief

The molecular mechanism behind the regulation of lipopolysaccharide synthesis regulation by LapB is currently unclear. Prince and Jia present the structure of LapB. LapB contains nine TPR motifs and a rubredoxin-type metal binding domain. The relationship between these structural motifs appears essential for function.

Highlights

- LapB contains nine TPR repeat motifs
- The rubredoxin metal binding domain is intimately bound to the TPR motifs
- Rubredoxin-TPR binding is essential for in vivo protein function

Accession Numbers

4ZLH

Prince and Jia, 2015, Structure *23*, 1500–1506
August 4, 2015
http://dx.doi.org/10.1016/j.str.2015.06.011

CellPress

Structure
Short Article

An Unexpected Duo: Rubredoxin Binds Nine TPR Motifs to Form LapB, an Essential Regulator of Lipopolysaccharide Synthesis

Chelsy Prince[1] and Zongchao Jia[1,*]
[1]Department of Biomedical and Molecular Sciences, Queen's University, Kingston, ON K7L3N6, Canada
*Correspondence: jia@queensu.ca
http://dx.doi.org/10.1016/j.str.2015.06.011

SUMMARY

Lipopolysaccharide (LPS) synthesis and export are essential pathways for bacterial growth, proliferation, and virulence. The essential protein LapB from *Escherichia coli* has recently been identified as a regulator of LPS synthesis. We have determined the crystal structure of LapB (without the N-terminal transmembrane helix) at 2 Å resolution using zinc single-wavelength anomalous diffraction phasing derived from a single bound zinc atom. This structure demonstrates the presence of nine tetratricopeptide repeats (TPR) motifs, including two TPR folds that were not predicted from sequence, and a rubredoxin-type metal binding domain. The rubredoxin domain is bound intimately to the TPR motifs, which has not been previously observed or predicted. Mutations in the rubredoxin/TPR interface inhibit in vivo cell growth, and in vitro studies indicate that these modifications cause local displacement of rubredoxin from its binding site without changing the secondary structure of LapB. LapB is the first reported structure to contain both a rubredoxin domain and TPR motifs.

INTRODUCTION

Interest in lipopolysaccharide (LPS) assembly protein B (LapB) began with two studies of the Keio collection of *Escherichia coli* single gene mutants where the *lapB* (previously known as *yciM*) knockout strain showed defects in biofilm formation and increased sensitivity to 21 different antibiotics (Baba et al., 2006; Liu et al., 2010; Tabe et al., 2007). Further investigation has revealed that *lapB* is an essential gene, and the Keio knockout mutant also contains a compensatory mutation in the *lpxC* gene (Mahalakshmi et al., 2014). Study of a *ΔlapB* suppressor-free strain showed extreme growth defects under laboratory conditions and elevated LPS, heterogeneous LPS, and accumulation of LPS precursors (Klein et al., 2014). LPS is a key component of the outer leaflet of the bacterial outer membrane found in most Gram-negative bacteria (Whitfield and Trent, 2014). LPS forms an innate permeability barrier that protects the cells from antibiotics, detergents, and dyes, due to the low fluidity of the LPS hydrocarbon domain and bridging of the negatively charged components of lipid A and the inner core sugar by divalent cations (Nikaido, 2003).

The regulation of LPS synthesis requires the degradation of the LpxC enzyme by the essential membrane bound protease FtsH (Führer et al., 2006). The LpxC enzyme catalyzes the first committed step of lipid A synthesis, and tight regulation of this enzyme is essential to cell survival (Ogura et al., 1999). More recently it has been shown that the degradation of LpxC is somehow mediated by LapB (Klein et al., 2014; Mahalakshmi et al., 2014). Direct binding between LapB and LpxC has not been observed, leaving the molecular mechanism behind LapB mediated degradation of LpxC unclear. The LapB protein has been pulled down with WaaC and LptD, which are also implicated in LPS biogenesis. This suggests that LapB may act as a central scaffold that coordinates the actions of various proteins in the LPS synthesis and export pathways (Klein et al., 2014).

LapB contains three major structural motifs: the N-terminal transmembrane helix, several tetratricopeptide repeats (TPR), and a C-terminal rubredoxin metal binding domain (Nicolaes et al., 2014). The N-terminal transmembrane helix anchors LapB to the inner membrane of Gram-negative bacteria with the soluble domain in the cytoplasm (Nicolaes et al., 2014).

TPR proteins are members of the solenoid family that contain helix-turn-helix folds with 34 amino acids each and a consensus sequence defined by a pattern of small and large hydrophobic residues (Karpenahalli et al., 2007; Kobe and Kajava, 2000). TPR motifs are most commonly found in groups of three consecutive repeats (Andrea et al., 2003). The structures of many TPR-containing proteins have been recently solved, including complexes with small molecules, peptides, or proteins bound to the concave face (Fodor et al., 2015; Pal et al., 2014; Wang et al., 2011).

Rubredoxin proteins form small non-heme iron binding sites that use four cysteine residues to coordinate a single metal ion in a tetrahedral environment. Rubredoxins are most commonly found in bacterial systems, but have also been found in eukaryotes (Chen et al., 2006; Schweimer et al., 2000). Examples of rubredoxin domains within larger proteins have also been identified. The key features of these rubredoxin-like domains are the extended loops or "knuckles" and the tetracysteine mode of iron binding (Bitto et al., 2008). Rubredoxins are usually implicated in redox reactions and electron transfer. Specific roles are known in a few systems, including n-alkane oxidation in *Pseudomonas aeruginosa* (Hagelueken et al., 2007), and an electron acceptor for CO dehydrogenase in *Acetobacterium woodii*

Table 1. Data Reduction, Experimental Phasing, Model Building, and Refinement Statistics for the Structure Determination of LapB

	SAD Phasing	Refinement
Dataset		
Space group	$P2_1$	
Unit cell dimensions	a = 38.31, b = 152.25, c = 65.47	
	α = 90.0, β = 93.91, γ = 90.0	
Wavelength (Å)	1.28292	
Resolution range (Å)	50–4.0 (4.1–4.0)	40.1–2.0 (2.1–2.0)
Unique reflections	12,429	97,844
I/sigma	63.74 (57.31)	11.01 (2.03)
Completeness (%)	100.0 (100.0)	98.1 (96.8)
Redundancy	21.2	3.15
R_{merge}	5.0 (5.5)	6.4 (66.4)
CC(1/2)	99.9 (99.9)	99.7 (68.2)
HySS figure of merit	0.498	
Refinement		
R_{work}/R_{free}		0.2056/0.2545
RMSD bond length (Å)		0.010
RMSD bond angles (°)		1.103
Clashscore		4.2
Ramachandran favored (%)		96.37
Ramachandran outliers (%)		0.15
Rotamer outliers (%)		0.43
No. of protein atoms		5,026
No. of solvent atoms		265

CC(1/2), percentage of correlation between intensities from random half-datasets; RMSD, root-mean-square deviation; SAD, single-wavelength anomalous diffraction.

(Ragsdale et al., 1983), but the exact role of rubredoxin and rubredoxin domains remains poorly understood in most systems (Chen et al., 2006).

Although the mechanism of LapB function remains unclear, it has been shown that both the metal binding rubredoxin and inner membrane localization of LapB are essential to the proper functioning of this regulator (Nicolaes et al., 2014). We have determined the structure of the LapB cytoplasmic domain to 2.0 Å by X-ray crystallography. The direct functional implications of this structure are discussed using mutation studies performed both in vitro and in vivo. LapB is the first protein to be structurally characterized that contains both TPR motifs and a rubredoxin domain.

RESULTS AND DISCUSSION

Optimized LapB and Crystallization

During initial trials, it was noted that LapB truncated to remove the N-terminal transmembrane helix (residues 19–389) could be expressed and purified as a soluble protein, but was prone to degradation that could be minimized by further truncation of the protein to residues 50–389. In addition, LapB was pink-orange in color, indicative of partial iron binding and consistent with parallel work that showed purified LapB bound to 20% iron and 80% zinc (Nicolaes et al., 2014). The metal binding properties of LapB were further explored by expressing LapB in minimal media and altering the availability of zinc ions. When extra zinc was provided, iron binding was significantly reduced and could not be detected by absorbance in the visible spectrum. In contrast, when zinc was removed, increased iron binding was observed, suggesting metal binding is competitive (Figure S1A). Zinc-bound centers are known to have increased stability over iron-bound centers (Petros et al., 2006), and it was zinc bound LapB that crystallized to form clusters of plates in space group $P2_1$ over a 3- to 8-week growth period (Figures S1B and S1C). The diffraction of crystals produced from LapB (50–389) was improved by approximately 1 Å in resolution over crystals grown from the LapB (19–389) construct. X-Ray data reduction, phasing, model building, and refinement statistics are listed in Table 1.

LapB Structure

Crystallized LapB is a dimer in the asymmetric unit with residues 67–389 in molecule A and residues 52–389 in molecule B (Figure 1A). Alignment of the two molecules demonstrates the same overall fold with a root-mean-square deviation of 1.29 Å, and backbone variation is mostly limited to the N-terminal TPR motifs. Analysis of this structure by PDBePISA (Krissinel and Henrick, 2007) suggests that this protein may form a biological dimer with an unusual ring shape (Figure 1B).

Sequence predictors, such as TPRpred, have identified seven TPR motifs from the LapB sequence (Karpenahalli et al., 2007). The second helix of the first repeat is seen in molecule B of the crystal structure and repeats 2–7 are present in both molecules (Figure 1C). The structure reveals two additional TPR motifs that were not predicted from sequence. Based on the structure of these folds, the sequences of repeats 8 and 9 can be aligned (Figure 2A). Repeats 8 and 9 have four conserved positions substituted, and there is one residue missing between repeats 8 and 9. Overall, most conserved positions still contain a hydrophobic residue, and these repeats form the same helix-turn-helix fold. Therefore, structure determination of LapB has revealed the presence of two additional TPR motifs with low sequence conservation.

Phyre2 structure prediction for LapB indicated several TPR motifs followed by a loosely associated rubredoxin domain (Kelley and Sternberg, 2009; Klein et al., 2014). This is consistent with the isolated nature of most rubredoxin proteins. However, the crystal structure of LapB reveals an extremely tight and unexpected binding of rubredoxin to nine highly organized TPR motifs. This interaction is mediated by two patches of contact, one dominated by large aromatic amino acids and the second dominated by electrostatic amino acids (Figure 3A). These patches are located on the concave face of TPR motifs 5–7, in agreement with previously identified TPR complexes (Fodor et al., 2015; Pal et al., 2014; Wang et al., 2011). This leaves additional binding space for proteins to dock to motifs 1–4 and motifs 7–9, consistent with the proposed role of LapB as a protein scaffold (Klein et al., 2014). Proteins docking to these locations on the concave face of the TPR motifs would also likely interact with the bound rubredoxin domain as a result of its central location (Figure 1A).

Isolated rubredoxin has a very well conserved fold, with ten nearly identical structures available from different organisms.

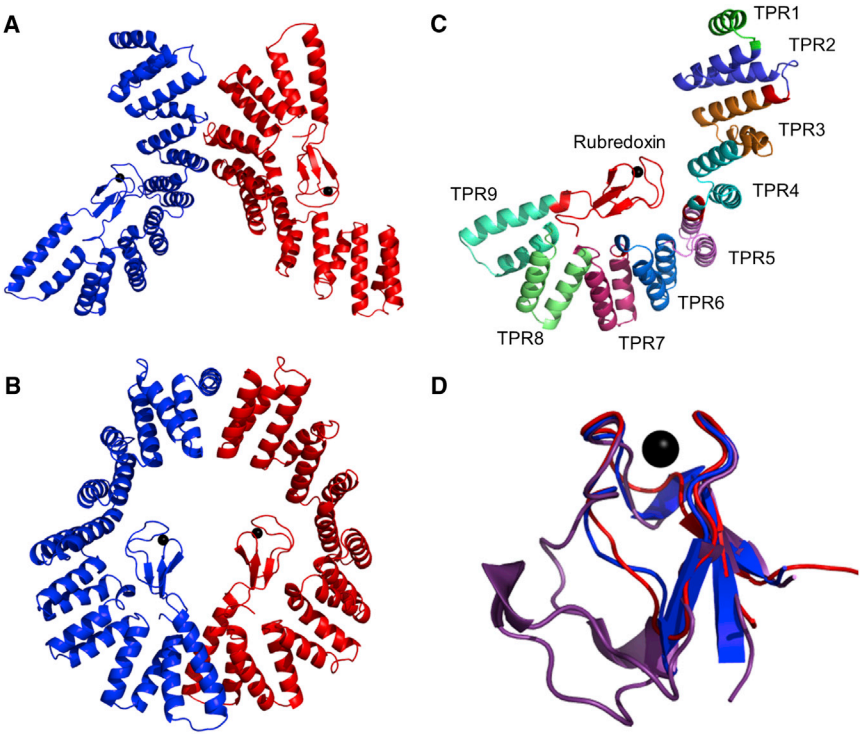

Figure 1. LapB Structure

(A) Cartoon diagram of the LapB dimer crystallized in the asymmetric unit.

(B) Cartoon diagram of the LapB ring dimer predicted by PDBePISA (Krissinel and Henrick, 2007).

(C) Monomer of LapB highlighting the position of the nine TPR motifs.

(D) Alignment of the rubredoxin domain (red) with representative models of isolated rubredoxin (purple: 7RXN) and the rubredoxin-like domain in rubrerythrin (blue: 1B71).

Bound zinc atoms are indicated by black spheres. Metal binding properties and representative crystals can be found in Figure S1.

The rubredoxin domain of LapB is more similar to the rubrerythrin family rubredoxin domain than isolated rubredoxins (Figure 1D). Rubrerythrin family proteins have been identified in air-sensitive bacteria, and contain a four-helix bundle with a diiron site and the rubredoxin domain (deMaré et al., 1996). Rubrerythrins have been implicated in the reduction of hydrogen peroxide, and the rubredoxin domain likely restores the reduced state of the diiron site post catalysis (Iyer et al., 2005). When the structure of LapB is compared with rubrerythrin it is noted that side chains of W369 and W377 from the aromatic patch are in positions occupied by much smaller side chains. In addition, K381 and R384 from the electrostatic patch at the C terminus align with hydrophobic residues in rubrerythrin (Figures 2B and 3A). This opens the possibility that these positions may have evolved to bind the TPR motifs. Overall, the TPR motifs have significant contact with the rubredoxin domain, covering 31.4% of its surface area (Lee and Richards, 1971).

Mutations in the TPR-Rubredoxin Interface Inhibit Cell Growth In Vivo

To enable the study of mutated LapB with the *ΔlapB* strain from the Keio collection, wild-type LpxC was overexpressed from a plasmid of low copy number. The introduction of wild-type LpxC has a dominant effect over the mutated LpxC expressed from the bacterial genome (mutation characterized by Mahalakshmi et al., 2014). This results in a sharp decrease in the cell growth rate for at least 8 hr, and is consistent with the growth defects observed in a suppressor-free *ΔlapB* strain (Klein et al., 2014) (Figure 3B). In addition, cell growth experiments were performed at 42°C to maximize the observed phenotype (Figure S2). To restore wild-type conditions a second plasmid for the expression of LapB is introduced, which regulates the overexpression of LpxC and restores wild-type growth conditions (Figure 3B). End point measurements were taken after 4 hr of growth in liquid culture, when both fast- and slow-growing strains are in optimal mid-log growth. A wide range of mutated *lapB* plasmids were introduced into this model system (Figure 3C). LapB mutants were also evaluated using a plating efficiency assay that provided comparable results (Figure S3).

Seven mutant strains exhibited less than 90% relative growth due to the inability of LapB to rescue the toxic overexpression of LpxC. A LapB truncation lacking the N-terminal transmembrane helix was unable to rescue cell growth, consistent with previous work showing that membrane localization is essential for LapB function (Nicolaes et al., 2014). Deletion of the entire rubredoxin domain was also shown to prevent cell growth, which confirms an important function for this domain. It has previously been shown that mutation of the four metal coordinating cysteines also causes a loss of function in vivo (Nicolaes et al., 2014). Finally, side-chain mutations including H181A, S378P, W369S/W377S, D244A/E246A/E250A, and D244A/E246A/E250A/E253A were identified as impairing growth and are presumed to cause a loss of function in the LapB protein, specifically the ability of rubredoxin to dock to the TPR superhelix. Notably, the growth defect of D244A/E246A/E250A was partially alleviated by additional mutation of L247 to glutamate, suggesting that a minimum of two negative residues are required in the electrostatic patch. Given that loss-of-function mutations were found on both the rubredoxin and the TPR faces of the interaction surfaces, we can propose that the specific binding of rubredoxin to the TPR helices is altered and that the docked state of rubredoxin plays a role in function.

LapB Mutants Are Folded

A wide selection of LapB mutations tested for cell growth in vivo were expressed and purified as soluble domains to assess the effect of the mutations on the structure of LapB. Mutated LapB showed recombinant expression in *E. coli* BL21 (DE3) equivalent to that of wild-type LapB, and could be purified in high yields using the same protocol. Notable exceptions were the W369S/W377S and D244A/E246A/E250A/E253A mutations, which had a large propensity to aggregate and precipitate at high concentration. It was determined by circular dichroism (CD)

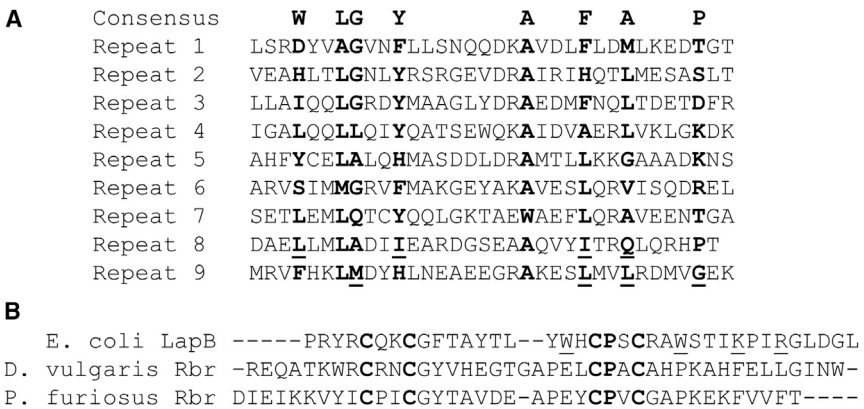

Figure 2. Sequence Alignments

(A) Alignment of the nine tetratricopeptide (TPR) repeats in LapB. Substitutions in repeats 8 and 9 are underlined.

(B) Alignment of the rubredoxin domain with rubrerythrin (Rbr). Poorly conserved residues are underlined.

spectroscopy that all single and double mutations do not affect the secondary structure of LapB (Figure 4A). The first mutant that showed a spectral change was the quadruple mutation of D244A/E246A/E250A/E253A, which potentially shows a slight loss of α-helical content. The concentration of this mutated protein was significantly decreased, and the apparent loss of secondary structure could also be an artifact of a decreased signal to noise ratio. Given the position of all four of these negative residues in the TPR repeats, it is possible that mutating more than three negative residues from this patch starts to disrupt the superhelical twist of the protein backbone (Figure 3A). Overall, mutation of five of these negative positions (D244A/E246A/E250A/E253A/N279A) was required before the protein became fully insoluble.

The rubredoxin deletion truncation was also expressed and purified to confirm that the TPR motifs could fold in the absence of rubredoxin. The CD spectrum of this truncation is consistent with the full-length protein, and although this truncation is more susceptible to degradation, it remains soluble. This confirms an essential role for the rubredoxin domain in the function of LapB that is independent of the folding of the TPR motifs.

LapB Mutants Alter Local Structure

Given the presence of three tryptophan residues (of four in LapB) in the TPR-rubredoxin interface, intrinsic tryptophan fluorescence was used to determine the tertiary folding of LapB in solution (Figure 4B). Wild-type LapB has an intrinsic tryptophan fluorescence peak of 332 nm, suggesting that all tryptophan residues are in a hydrophobic environment. In addition, tryptophan fluorescence was observed after LapB was incubated with a crosslinker (glutaraldehyde). If the rubredoxin domain is mobile, we would expect the crosslinker to "lock" the protein in the bound state and cause a significant change in fluorescence. Only a small 1-nm shift in fluorescence was observed for crosslinked LapB. Therefore, the tightly bound conformation of rubredoxin observed in the LapB crystal structure also occurs in solution (Figure 4B).

Loss-of-function mutants H181A and S378P both cause an upward shift in the wavelength of tryptophan fluorescence, consistent with a more hydrophilic tryptophan environment and weaker rubredoxin-TPR binding (Figure 4B). H181 is central to the aromatic patch on the TPR face, and mutation of this single residue is enough to cause a growth defect. Mutation of both W369 and W377 in the rubredoxin domain was required to produce a similar cell growth defect. S378P also shows a significant fluorescence shift, and CD spectroscopy confirms that there is no major loss of protein folding. The mutation to proline more likely causes a local disruption in structure that moves the neighboring tryptophan residues into less favorable positions for binding.

In contrast, tryptophan fluorescence indicates that mutation of K381A and K381A/R384A causes a shift to a more hydrophobic environment (Figure 4B). This would suggest tighter packing of the rubredoxin into the TPR helices. It is possible that nearby R354 could bind the negative region of the TPR motifs, resulting in a counterclockwise rotation of rubredoxin that is consistent with tighter packing at the aromatic patch. Given that H181A and S378P both cause a reduction in cell growth while mutations of K381 and R384 do not have an effect, it can be concluded that tight packing of rubredoxin to the TPR motifs is necessary for the function of LapB.

Conclusion

The LapB regulator contains an unprecedented combination of TPR motifs and rubredoxin. Structure determination has revealed two additional TPR motifs that were not predicted due to poorly conserved sequences and an unexpected binding of rubredoxin to the concave face of the TPR superhelix. The rubredoxin domain has an important structural role, and its association to the TPR motifs is essential to LPS regulation. The molecular mechanism of the down-regulation of LpxC by LapB remains unclear, but could involve both the scaffold-type binding typical of TPR motifs and the redox activity of the rubredoxin domain. A greater understanding of LPS regulation will aid in the development of future pharmaceuticals targeting Gram-negative bacterial pathogens.

EXPERIMENTAL PROCEDURES

Protein Expression and Purification of Soluble LapB

The *lapB* gene was amplified from *E. coli* K12 and inserted into a modified pET32a expression plasmid to express a soluble construct of HisTag-Thioredoxin-HisTag-TEV_Site-LapB. Protein was expressed in BL21 cells using auto-induction media (Studier, 2005). Cells were harvested by centrifugation at 3,300 × *g* and re-suspended in 25 ml of lysis buffer (50 mM Na_2HPO_4, 300 mM NaCl, 0.1% Triton X-100, 1 mg/ml lysozyme). Cells were lysed by sonication and lysate clarified by centrifugation (21,000 × *g*) was mixed with 3 ml of Ni-agarose resin. Resin was washed and eluted by gravity with 0, 30, 60, 90, and 300 mM imidazole in wash buffer (50 mM Na_2HPO_4, 250 mM NaCl). Protein was cleaved with TEV protease overnight (1:10 protease/protein) at 4°C and run on a Superdex 200 size-exclusion column (GE). LapB is eluted as a single peak that is well separated from TEV/thioredoxin.

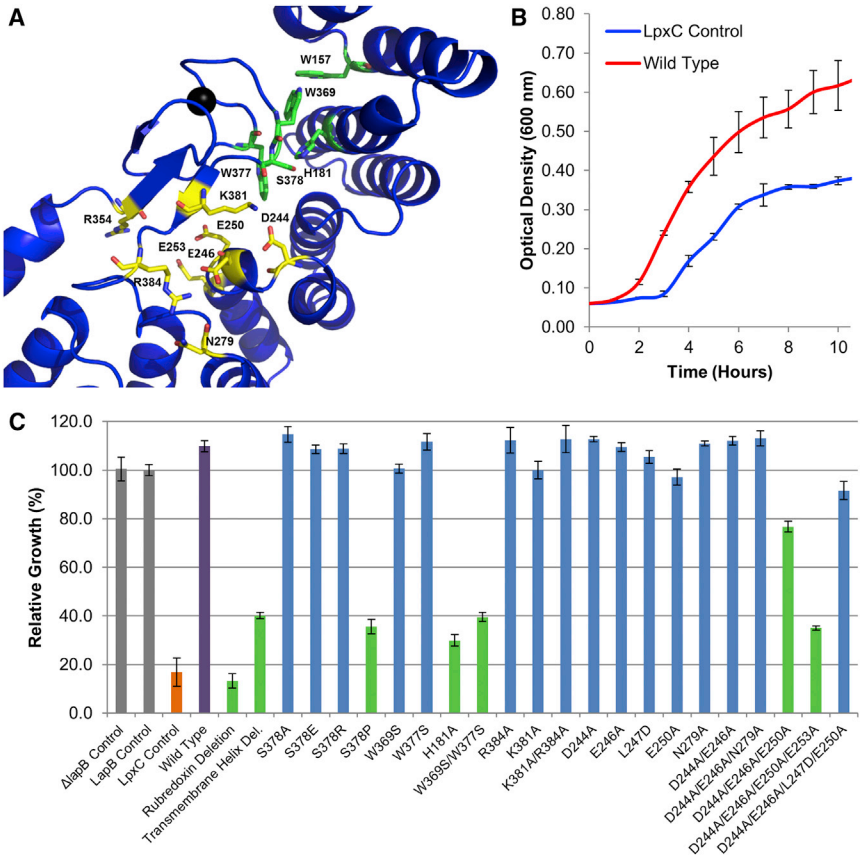

Figure 3. Rubredoxin-TPR Binding Interface

(A) Binding of rubredoxin to the TPR motifs. Residues in the aromatic region (green) and the electrostatic region (yellow) are displayed as sticks. Bound zinc atom is indicated by a black sphere.

(B) Growth of *E. coli* at 42°C during expression of wild-type LpxC and during expression of both LpxC and LapB. Growth of these strains at 20°C and 37°C is plotted in Figure S2.

(C) Rescue of LpxC overexpression by LapB. *ΔlapB* Control is the *lapB* knockout strain transformed with pDL804 and pMS604 for antibiotic resistance, and expresses neither protein. LapB and Control and LpxC Control (gray) contain one protein expression plasmid and pDL804 or pMS604 as required for antibiotic resistance. LpxC Control (orange) shows the expected growth defect. Rescue of LpxC overexpression is achieved by wild-type LapB (purple) and some LapB mutants (blue). Mutant LapB proteins incapable of rescuing the growth defect are shown in green. A comparable plating efficiency assay was also performed (Figure S3).

Data are plotted as the average and SD of triplicate measurements.

Crystallization and X-Ray Diffraction

Soluble LapB truncations (5–10 mg/ml) were crystallized by hanging-drop vapor diffusion at 20°C with 0.2 M $(NH_4)_2SO_4$, 25% PEG 3350, and 0.1 M Bis-Tris (pH 6.5) over a period of 3–8 weeks. Individual crystals were harvested after addition of 20%–30% glycerol to drops covered with 15 μl of mineral oil. X-Ray diffraction data were collected at the 23-IDB GMAT beamline at the Advance Photon Source. Eight datasets with 200–360 frames each were collected using a micro-focused beam to collect five datasets from different areas of the first crystal and three datasets from a second crystal.

Data Reduction and Model Building

All datasets were integrated and merged using the XDS package (Kabsch, 2010). Zinc positions were determined using HySS (Grosse-Kunstleve and Adams, 2003) and the merged datasets truncated to 4.0 Å. Phases were extended using Phaser (McCoy et al., 2007). The correct hand was chosen by using RESOLVE density modification (Terwilliger, 2003). The initial model was built using the Autobuild and the Phase_and_build wizards in PHENIX (Terwilliger et al., 2007). Model building was performed in Coot (Emsley and Cowtan, 2004). Constraints for the metal binding site were defined using ReadySet, and phenix.refine was used for refinement (Afonine et al., 2012). Molecular figures were prepared using PyMOL (Schrödinger, LLC, 2010). Data have been deposited in the PDB (PDB: 4ZLH).

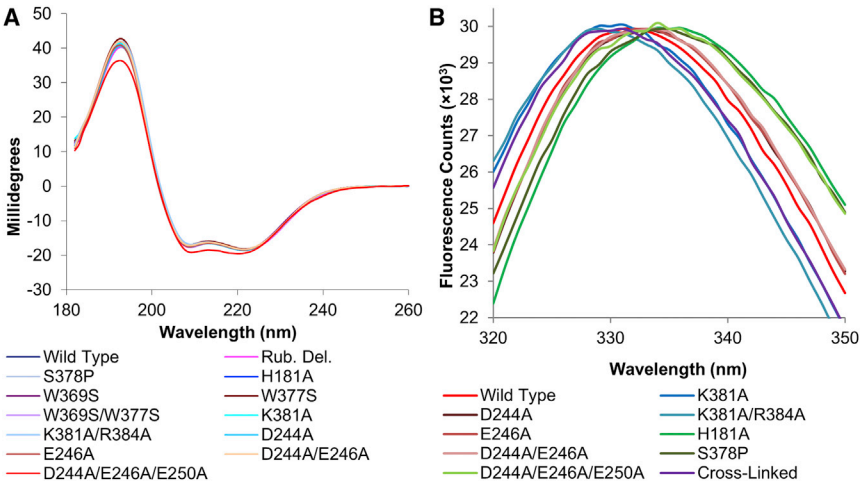

Figure 4. In Vitro Studies

(A) Circular dichroism spectra of LapB mutations overlay extremely well, indicating consistent folding of the TPR α helices. Rub. Del., rubredoxin deletion.

(B) Intrinsic tryptophan fluorescence of mutant LapB proteins. Purple, crosslinked protein with peak wavelength of 331 nm; blue, mutants that have a peak wavelength lower than 332 nm; red, wild-type and mutants that have a peak wavelength of 332–333 nm; green, mutants that have a peak wavelength of 325 nm.

Plasmid Construction

Two plasmids with a lacUV5 promoter, pDL804 and pMS604 (Dmitrova et al., 1998), were provided by Dr. Keith Poole (Queen's University) and are ampicillin and tetracycline resistant, respectively. These vectors were modified to express full-length LapB and LpxC proteins with no additional residues. Single amino acid mutations were made in the LapB gene using Quick-Change site-directed mutagenesis (Stratagene) with 4% DMSO added to the PCR reactions. Multiple mutations were introduced simultaneously using overlap extension PCR (Ho et al., 1989). All mutations were confirmed by DNA sequencing.

Bacterial Strains and Growth Conditions

The Δ*lapB E. coli* strain (JW1272) was obtained from the Keio collection (Baba et al., 2006). The pDL804 and pMS604 vectors were transformed into the Δ*lapB* strain to generate the *ΔlapB* control, which has resistance to ampicillin and tetracycline. The pDL804-*lpxC* plasmid was transformed into JW1272 with wild-type or mutant LapB plasmids to create experimental strains (Table S1). In all cases, picked colonies were grown overnight in 5 ml of LB media supplemented with 100 μg/ml ampicillin and 10 μg/ml tetracycline. The optical density (OD) of each culture at 600 nm was adjusted to 0.5, and 300 μl of cells was used to start fresh 5-ml LB cultures supplemented with both antibiotics and 0.5 mM isopropyl β-D-1-thiogalactopyranoside. 300 μl of cells was removed to measure OD in a 96-well plate at each time point. Cells were grown at 20°C, 37°C, or 42°C with shaking at 225 rpm. Growth of the wild-type strain (CCP104) was used as the reference for 100% cell growth after 4 hr. The remaining LapB mutants were evaluated by calculating their growth relative to this standard as a percent. An additional colony-forming assay was performed, the methods and results of which are given in the Supplemental Information.

Tryptophan Fluorescence

Intrinsic tryptophan fluorescence was measured using a Fluorolog Tau-3 Lifetime Fluorimeter (Jobin Yvon Horiba) from a 100-μl sample at 20 μM. Thirty scans were collected between 320 and 350 nm using an excitation wavelength of 295 nm and a bandpass of 1 nm. Curves are presented after averaging and normalization. Crosslinked protein was tested by separating a single 23-μM sample and incubating half the sample with 1% glutaraldehyde overnight.

CD Spectroscopy

CD data were collected using a Chirascan spectrometer (Applied Photophysics) and a 200-μl protein sample at a concentration of 20 μM in 20 mM Tris (pH 8.0) and 150 mM NaF. The path length of the cell was 0.1 mM, and spectra were collected between 182 and 260 nm. Three scans were collected from each sample and averaged. Final spectra are presented after subtraction of an appropriate blank and normalization.

ACCESSION NUMBERS

Data on the structure of LapB have been deposited in the PDB (PDB: 4ZLH).

SUPPLEMENTAL INFORMATION

Supplemental Information includes Supplemental Methods, three figures, one table, 3D molecular models, and PDB Validation Report and can be found with this article online at http://dx.doi.org/10.1016/j.str.2015.06.011.

AUTHOR CONTRIBUTIONS

C.P. designed and executed the experiments, analyzed the data, and prepared the manuscript. Z.J. was the primary supervisor of this work and provided advice at all stages.

ACKNOWLEDGMENTS

We would like to thank the beamline staff at GMAT (Advance Photon Source) for assistance with data collection. Tryptophan fluorescence and CD spectra were collected with the assistance of Kim Munro at the Protein Function Discovery Facility (Queen's University). Z.J. is a Canada Research Chair in Structural Biology and C.P. holds a Frederick Banting and Charles Best Canada Graduate Scholarship. Research funding was provided by the Canadian Institutes of Health Research and the Natural Sciences and Engineering Research Council of Canada.

Received: May 6, 2015
Revised: June 11, 2015
Accepted: June 11, 2015
Published: July 16, 2015

REFERENCES

Afonine, P.V., Grosse-Kunstleve, R.W., Echols, N., Headd, J.J., Moriarty, N.W., Mustyakimov, M., Terwilliger, T.C., Urzhumtsev, A., Zwart, P.H., and Adams, P.D. (2012). Towards automated crystallographic structure refinement with phenix.refine. Acta Crystallogr. D Biol. Crystallogr. *68*, 352–367.

Andrea, L.D.D., Regan, L., and D'Andrea, L. (2003). TPR proteins: the versatile helix. Trends Biochem. Sci. *28*, 655–662.

Baba, T., Ara, T., Hasegawa, M., Takai, Y., Okumura, Y., Baba, M., Datsenko, K.A., Tomita, M., Wanner, B.L., and Mori, H. (2006). Construction of *Escherichia coli* K-12 in-frame, single-gene knockout mutants: the Keio collection. Mol. Syst. Biol. *2*, 1–11.

Bitto, E., Bingman, C.A., Bittova, L., Kondrashov, D.A., Bannen, R.M., Fox, B.G., Markley, J.L., and Phillips, G.N. (2008). Structure of human J-type co-chaperone HscB reveals a tetracysteine metal-binding domain. J. Biol. Chem. *283*, 30184–30192.

Chen, C.J., Lin, Y.H., Huang, Y.C., and Liu, M.Y. (2006). Crystal structure of rubredoxin from *Desulfovibrio gigas* to ultra-high 0.68 A resolution. Biochem. Biophys. Res. Commun. *349*, 79–90.

deMaré, F., Kurtz, D.M., and Nordlund, P. (1996). The structure of *Desulfovibrio vulgaris* rubrerythrin reveals a unique combination of rubredoxin-like FeS4 and ferritin-like diiron domains. Nat. Struct. Biol. *3*, 539–546.

Dmitrova, M., Younès-Cauet, G., Oertel-Buchheit, P., Porte, D., Schnarr, M., Granger-Schnarr, M., and Youne, M.D.G. (1998). A new LexA-based genetic system for monitoring and analyzing protein heterodimerization in *Escherichia coli*. Mol. Gen. Genet. *257*, 205–212.

Emsley, P., and Cowtan, K. (2004). Coot: model-building tools for molecular graphics. Acta Crystallogr. D Biol. Crystallogr. *60*, 2126–2132.

Fodor, K., Wolf, J., Reglinski, K., Passon, D.M., Lou, Y., Schliebs, W., Erdmann, R., and Wilmanns, M. (2015). Ligand-induced compaction of the PEX5 receptor-binding cavity impacts protein import efficiency into peroxisomes. Traffic *16*, 85–98.

Führer, F., Langklotz, S., and Narberhaus, F. (2006). The C-terminal end of LpxC is required for degradation by the FtsH protease. Mol. Microbiol. *59*, 1025–1036.

Grosse-Kunstleve, R.W., and Adams, P.D. (2003). Substructure search procedures for macromolecular structures. Acta Crystallogr. D Biol. Crystallogr. *59*, 1966–1973.

Hagelueken, G., Wiehlmann, L., Adams, T.M., Kolmar, H., Heinz, D.W., Tümmler, B., and Schubert, W.-D. (2007). Crystal structure of the electron transfer complex rubredoxin rubredoxin reductase of *Pseudomonas aeruginosa*. Proc. Natl. Acad. Sci. USA *104*, 12276–12281.

Ho, S.N., Hunt, H.D., Horton, R.M., Pullen, J.K., and Pease, L.R. (1989). Site-directed mutagenesis by overlap extension using the polymerase chain reaction. Gene *77*, 51–59.

Iyer, R.B., Silaghi-Dumitrescu, R., Kurtz, D.M., and Lanzilotta, W.N. (2005). High-resolution crystal structures of *Desulfovibrio vulgaris* (Hildenborough) nigerythrin: facile, redox-dependent iron movement, domain interface variability, and peroxidase activity in the rubrerythrins. J. Biol. Inorg. Chem. *10*, 407–416.

Kabsch, W. (2010). XDS. Acta Crystallogr. D Biol. Crystallogr. *66*, 125–132.

Karpenahalli, M.R., Lupas, A.N., and Söding, J. (2007). TPRpred: a tool for prediction of TPR-, PPR- and SEL1-like repeats from protein sequences. BMC Bioinformatics *8*, 2.

Kelley, L.A., and Sternberg, M.J.E. (2009). Protein structure prediction on the Web: a case study using the Phyre server. Nat. Protoc. *4*, 363–371.

Klein, G., Kobylak, N., Lindner, B., Stupak, A., and Raina, S. (2014). Assembly of lipopolysaccharide in *Escherichia coli* requires the essential LapB heat shock protein. J. Biol. Chem. *289*, 14829–14853.

Kobe, B., and Kajava, A.V. (2000). When protein folding is simplified to protein coiling: the continuum of solenoid protein structures. Trends Biochem. Sci. *25*, 509–515.

Krissinel, E., and Henrick, K. (2007). Inference of macromolecular assemblies from crystalline state. J. Mol. Biol. *372*, 774–797.

Lee, B., and Richards, F.M. (1971). The interpretation of protein structures: estimation of static accessibility. J. Mol. Biol. *55*, 379–400.

Liu, A., Tran, L., Becket, E., Lee, K., Chinn, L., Park, E., Tran, K., and Miller, J.H. (2010). Antibiotic sensitivity profiles determined with an *Escherichia coli* gene knockout collection: generating an antibiotic bar code. Antimicrob. Agents Chemother. *54*, 1393–1403.

Mahalakshmi, S., Sunayana, M.R., SaiSree, L., and Reddy, M. (2014). yciM is an essential gene required for regulation of lipopolysaccharide synthesis in *Escherichia coli*. Mol. Microbiol. *91*, 145–157.

McCoy, A.J., Grosse-Kunstleve, R.W., Adams, P.D., Winn, M.D., Storoni, L.C., and Read, R.J. (2007). Phaser crystallographic software. J. Appl. Crystallogr. *40*, 658–674.

Nicolaes, V., El Hajjaji, H., Davis, R.M., Van der Henst, C., Depuydt, M., Leverrier, P., Aertsen, A., Haufroid, V., Ollagnier de Choudens, S., De Bolle, X., et al. (2014). Insights into the function of YciM, a heat shock membrane protein required to maintain envelope integrity in *Escherichia coli*. J. Bacteriol. *196*, 300–309.

Nikaido, H. (2003). Molecular basis of bacterial outer membrane permeability revisited. Microbiol. Mol. Biol. Rev. *67*, 593–656.

Ogura, T., Inoue, K., Tatsuta, T., Suzaki, T., Karata, K., Young, K., Su, L.H., Fierke, C.A., Jackman, J.E., Raetz, C.R.H., et al. (1999). Balanced biosynthesis of major membrane components through regulated degradation of the committed enzyme of lipid A biosynthesis by the AAA protease FtsH (HflB) in *Escherichia coli*. Mol. Microbiol. *31*, 833–844.

Pal, M., Morgan, M., Phelps, S.E.L., Roe, S.M., Parry-Morris, S., Downs, J.A., Polier, S., Pearl, L.H., and Prodromou, C. (2014). Structural basis for phosphorylation-dependent recruitment of Tel2 to Hsp90 by Pih1. Structure *22*, 805–818.

Petros, A.K., Reddi, A.R., Kennedy, M.L., Hyslop, A.G., and Gibney, B.R. (2006). Femtomolar Zn(II) affinity in a peptide-based ligand designed to model thiolate-rich metalloprotein active sites. Inorg. Chem. *45*, 9941–9958.

Ragsdale, S.W., Ljungdahl, L.G., and DerVartanian, D.V. (1983). Isolation of carbon monoxide dehydrogenase from *Acetobacterium woodii* and comparison of its properties with those of the *Clostridium thermoaceticum* enzyme. J. Bacteriol. *155*, 1224–1237.

Schrödinger, LLC. (2010). The {PyMOL} Molecular Graphics System, Version∼1.3r1 (Schrödinger, LLC).

Schweimer, K., Hoffmann, S., Wastl, J., Maier, U.G., Rösch, P., and Sticht, H. (2000). Solution structure of a zinc substituted eukaryotic rubredoxin from the cryptomonad alga *Guillardia theta*. Protein Sci. *9*, 1474–1486.

Studier, F.W. (2005). Protein production by auto-induction in high-density shaking cultures. Protein Expr. Purif. *41*, 207–234.

Tabe, E., Iba, E.N., Aka, Y.N., Agase, M.N., Ori, H.M., and Itakawa, M.K. (2007). A genome-wide approach to identify the genes involved in biofilm formation in *E. coli*. DNA Res. *14*, 237–246.

Terwilliger, T.C. (2003). SOLVE and RESOLVE: automated structure solution and density modification. Methods Enzymol. *374*, 22–37.

Terwilliger, T.C., Grosse-Kunstleve, R.W., Afonine, P.V., Moriarty, N.W., Zwart, P.H., Hung, L.W., Read, R.J., and Adams, P.D. (2007). Iterative model building, structure refinement and density modification with the PHENIX AutoBuild wizard. Acta Crystallogr. D Biol. Crystallogr. *64*, 61–69.

Wang, L., Liu, Y.T., Hao, R., Chen, L., Chang, Z., Wang, H.R., Wang, Z.X., and Wu, J.W. (2011). Molecular mechanism of the negative regulation of Smad1/5 protein by carboxyl terminus of Hsc70-interacting protein (CHIP). J. Biol. Chem. *286*, 15883–15894.

Whitfield, C., and Trent, M.S. (2014). Biosynthesis and export of bacterial lipopolysaccharides. Annu. Rev. Biochem. *83*, 99–128.

